Fourth International Symposium on Marine Propulsors
smp'15, Austin, Texas, USA, June 2015

# A Full Scale CFD Analysis of the Twin Fin Propulsion System

**Tobias Huuva[1], Simon Törnros[1]**

[1] Caterpillar Propulsion Production AB
Andvägen 26, SE-475 40 Hönö, Sweden

## ABSTRACT

The Twin Fin propulsion system consists of a rudder, propeller, short shafting and an electrical motor placed in a hydrodynamic shaped fin mounted under the hull. The flexible design of the fins allows a much larger propeller diameter than other common propulsion systems such as azimuth thrusters. The hydrodynamics of the propulsion system is analyzed using empirical data and computational fluid dynamics. Empirical data is used to show how a larger diameter affects the thrust for a highly loaded propeller at constant power. CFD is employed using an in-house modified solver based on the finite volume library OpenFOAM 2.3 to study the inflow to the propeller, the load variation, cavitation and thrust deduction.

### Keywords

Twin Fin, Full scale, CFD, Towing, Propeller, Wake, Thrust deduction, OpenFOAM, Cavitation

## 1 INTRODUCTION

Today diesel-electric propulsion systems are most commonly equipped with rotatable thrusters, utilizing mechanical or podded drives. This eliminates the need for rudder and stern tunnel thrusters, but makes the vessel more vulnerable due to high complexity and moving mechanical parts not being accessible from inside the vessel. In case of break down on these units it is normally necessary to go in dry dock for repair.

An alternative to azimuth thrusters is a conventional setup with long shafts, stern tube and machinery positioned inside the hull. This system is more reliable than azimuth thrusters, but requires more space for gear and electric motor in parts of the ship where cargo or other type of equipment can be placed. With the new Twin Fin concept, the advantages of both these setups can be combined. Two separate propulsion units substitutes the thrusters, these consist of a rudder, propeller, short shafting and an electrical motor placed in a hydrodynamic shaped fin mounted under the hull.

Using a CP propeller, with or without a nozzle and a flap type rudder, results in high maneuverability and flexibility. The flexible design of the fin makes it possible to fit a much larger propeller than using the other solutions, granting highly improved propulsive efficiency in many conditions, especially close to bollard pull (Huuva, 2014). The fins can also be designed to include more equipment, such as redundancy motors and similar, for improved accessibility.

The Twin Fin propulsion system can easily be retrofitted, see Figure 1 for a practical application of retrofitting the Twin Fin propulsion system.

**Figure 1 The Twin Fin propulsion system applied on a similar vessel**

The purpose of this study is to perform a numerical full scale analysis of the hydrodynamic performance of the Twin Fin Propulsion System. The main emphasis of the study is focused on the inflow to the propeller, propeller loading, cavitation and towing capability. The hull form used is of typical offshore support vessel (OSV) type equipped with twin nozzle propellers, see Figure 2.

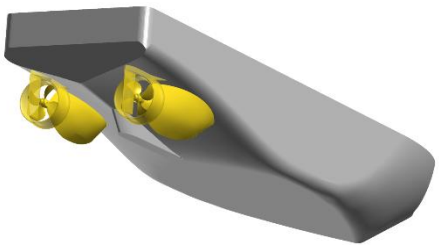

**Figure 2 Twin Fin propulsion system and hull 3D geometries**

Properties of the vessel is shown in Table 1.

**Table 1 Vessel properties**

| | | | |
|---|---|---|---|
| Length between perpendiculars | $L_{PP}$ | [m] | 86 |
| Breadth | B | [m] | 19 |

| | | | |
|---|---|---|---|
| Draught | T | [m] | 6.6 |
| Propeller diameter | D | [m] | 4.5 |
| Deliviered power | $P_D$ | [MW] | 3.5 |

The port side fin can be seen in Figure 3. Note that the hull longitudinal direction is to the left in the picture, looking at the portside fin from outside (Y-) and beneath (Z+) the vessel. The fins are 15.35 m long with an area of 131.5 $m^2$ per fin.

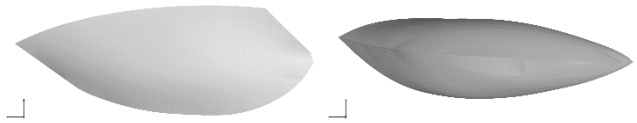

**Figure 3 3D geometry of the portside fin**

The analysis is performed in full scale to take full advantage of computational fluid dynamics in comparison to experimental fluid dynamics, where scale effects would have been inevitable. The free surface is considered using the Volume Of Fluid (VOF) method by an in-house modified solver originating from the C++ finite volume library OpenFOAM 2.3. Turbulence is modelled using Unsteady Reynolds Averaged Navier Stokes (URANS). Large Eddy Simulation (LES) has shown ability of resolving more details than URANS for cavitating flows, however URANS requires a significantly lower computational effort which makes URANS a suitable approach for industrial CFD for cavitating flows. Cavitation is taken into account by using the mass transfer model by Kunz et al. (1999).

The propulsion system is investigated at two speeds, low speed of 5 knots (towing mode) where this type of vessel operates most of the time and at high speed (free running condition) of 15 knots. The Reynolds number is high for both vessel speeds while the Froude number hints about high wave making resistance in free running speed only, see Table 2.

**Table 2 Velocities and corresponding Reynolds number and Froude number**

| $V_S$ [kn] | Re [-] | Fn [-] |
|---|---|---|
| 5 | 2E+8 | 0.088 |
| 15 | 6E+8 | 0.265 |

## 2 FORMULATION

### 2.1 Solver

The in-house modified solver is based on the C++ finite volume library OpenFOAM 2.3. The solver is a multiphase solver, taking two fluids into account using the Volume Of Fluid (VOF) approach. The solver utilizes the semi-implicit Multidimensional Universal Limited with Explicit Solution (MULES) to allow for higher courant numbers and still maintain boundedness.

### 2.2 Governing equations

The governing equation for the CFD problems are described by the Reynolds averaged Navier Stokes equation and Boussinesq assumption.

$$\frac{\partial \rho \boldsymbol{U}}{\partial t} + \boldsymbol{U} \cdot \nabla(\rho \boldsymbol{U}) = \nabla \cdot \left((\mu + \mu_t)\nabla \boldsymbol{U}\right) - \nabla p$$

Note that surface tension is not included. The turbulent viscosity $\mu_t$ needs to be modelled using a turbulence model. The RANS turbulence model k-ω SST was used together with wall functions.

The transport equation for mass (continuity equation)

$$\nabla \cdot \boldsymbol{U} = S_p$$

Note that the source term $S_p$ on the right hand side appears due to mass transfer in case of cavitation. If cavitation is not regarded then this term is zero and the flow is divergence free. When cavitation is present, the source term is computed by the following

$$S_p = \dot{m}\left(\frac{1}{\rho_l} - \frac{1}{\rho_v}\right)$$

The transport equation for the liquid volume fraction can be written

$$\frac{\partial \alpha}{\partial t} + \boldsymbol{U} \cdot \nabla \alpha = \frac{\dot{m}}{\rho_l}$$

The mass transfer term $\dot{m}$ appearing in the source term in the continuity equation and in the transport equation for the liquid volume fraction needs to be modelled by a cavitation model. The fluid properties in Table 3 were used throughout the study.

**Table 3 Fluid properties**

| | | | |
|---|---|---|---|
| Water density | $\rho_{water}$ | [$kgm^{-3}$] | 1025 |
| Water kinematic viscosity | $\nu_{water}$ | [$m^2s^{-1}$] | 1.11E-6 |
| Air density | $\rho_{water}$ | [$kgm^{-3}$] | 1.2 |
| Air kinematic viscosity | $\nu_{water}$ | [$m^2s^{-1}$] | 1.48E-5 |
| Vaporization pressure | $P_{vap}$ | [kPa] | 2.33 |
| Far-field air pressure | $P_{atm}$ | [kPa] | 101.325 |

### 2.3 Cavitation model

The pressure driven model developed by Kunz is used due to prior experience and successful simulations of cavitating propeller flows as shown by Huuva(2008) and Törnros(2013). In this model the vaporization and condensation are treated separately.

$$\dot{m} = \dot{m}^+ + \dot{m}^-$$

The vaporization term $\dot{m}^+$ is active when the pressure is lower than the vaporization pressure and depends on the liquid volume fraction to avoid negative volume fraction values.

$$\dot{m}^+ = \left(\frac{C_{prod}}{U_\infty^2 t_\infty}\right)\frac{\rho_v}{\rho_l}\alpha \min[0, p - p_v]$$

The condensation term $\dot{m}^-$ on the other hand is always present where there is mixture, independently of the pressure. The condensation term has its maximum where the liquid volume fraction is 2/3.

$$\dot{m}^- = \left(\frac{C_{dest}}{t_\infty}\right)\rho_v\alpha^2[1-\alpha]$$

Including cavitation as well as the air and water means that three different fluids are present. The current solver and setup only allows two fluids to be included in the simulation. To deal with this obstacle, the vapor is given the same fluid properties as air, reducing the number of fluids to two. This however means that the following discrepancies are included. First, the cavitation will behave as air rather than vaporous water. Secondly, the condensation term in the mass transfer model by Kunz is always active in mixture regions meaning that condensation will appear on the free surface. The model constants for the Kunz cavitation model can be seen in Table 4.

**Table 4 Kunz cavitation model constants**

| | |
|---|---|
| $\frac{C_{prod}}{U_\infty^2 t_\infty}$ | 425 |
| $\frac{C_{dest}}{t_\infty}$ | 30 |

### 2.4 Rotor modelling

The rotating propeller is modelled using sliding mesh. The mesh is a composition of two meshes, one stator and one rotor. The rotor contains the rotating propeller and the inside of the nozzle which is modelled as static through its boundary conditions. The interfaces between the rotor and the stator mesh volumes uses Arbitrary Mesh Interface (AMI) which allows simulation across unmatched and unconnected patches. Although the present propeller is controllable pitch, it is operated as a fixed pitch with the pitch setting equal to its design pitch.

### 2.5 Discretization

The static volume is meshed using the utility snappyHexMesh which is distributed within the OpenFOAM-package. The mesh is made by hex-like elements and is anisotropically refined (vertically) near the free surface as the wave length is assumed higher than the wave height. Only the port side of the ship is included in the simulations, to take advantage of the symmetrical problem. The mesh on the symmetryplane can be seen in Figure 4.

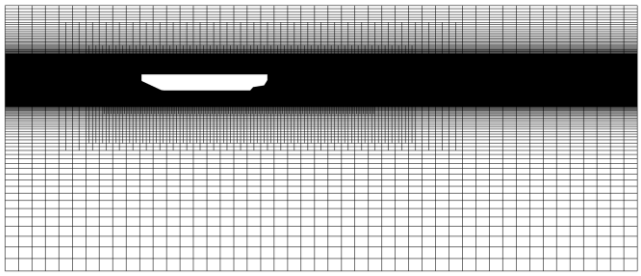

**Figure 4 Mesh on symmetryplane**

The rotating mesh volume, containing propeller, hub and inside of the nozzle is discretized into 3.7 million polyhedrals. Polyhedrals are used due to the many faces which are beneficial for rotating flows as it is difficult to align the mesh with the flow. The total size of the meshes ranges from 8.5 to 13.5 million cells. In Figure 5 the static Hex-like mesh is shown in blue and the rotating polyhedral mesh in red.

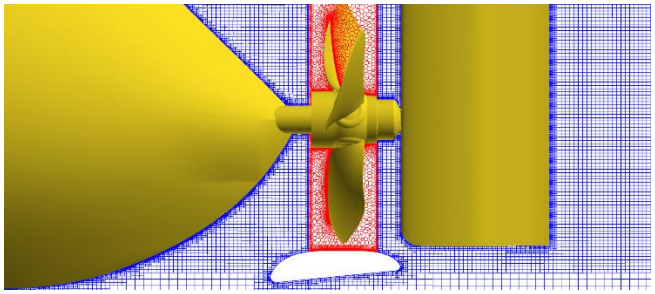

**Figure 5 Rotating (red) and static (blue) mesh volumes**

The near wall discretization is coarser than optimal, with average $Y^+$ values in 5 knots of 160 on the blades, 250 on the fin and 590 on the hull. Second order schemes are used for the convection terms, except for the turbulent quantities which together with the time discretization utilizes first order schemes.

## 3 RESULTS AND DISCUSSION

### 3.1 Validation

Separate components of the current problem has been validated. These are the open water propeller performance (Klerebrant Klasson, 2011), cavitation simulation on propellers using RANS (Törnros, 2013) and ship resistance prediction using non-public test cases. The current work combines these capabilities to study the full scale hydrodynamics including cavitating propeller flow when operating in behind condition including the free surface. Note that the unconventional numerical approach for the cavitating condition is not validated and results are shown “as is”.

### 3.2 Open water gains

The simple shaft configuration with a short shaft and less moving mechanical parts (“90° gears”) allows large torque and thereby large propeller diameter and low rotational speed. The Wageningen CD-series shows that the increased diameter, example 3.5 to 4.5 m increases the bollard pull

thrust by roughly 23% and towing thrust by 16% for the same delivered power, Figure 6. This is expected for a highly loaded propeller as a larger diameter reduces the induced axial velocities. In addition to this, the simple power transfer from the engine to the propeller will also have significantly better mechanical efficiency in comparison to many alternative propulsion solutions such as azimuth units which would increase the thrust even more.

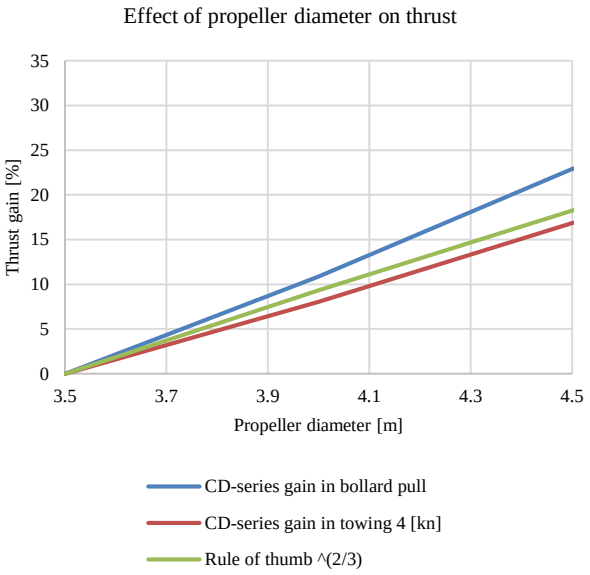


**Figure 6 Thrust dependence on propeller diameter**

### 3.2 Added resistance due to the fins

To find the added resistance due to the fins, resistance was computed for two barehulls, including and excluding the fins. The fins adds 8% to the wetted surface which is expected to increase the total flat plate friction while the form effects and especially the effect of the fins on the wave making resistance needs to be investigated. The effect on wave making resistance is of course hull dependent. Note that the rudder is considered to be a part of the hull rather than the propulsion system. The added resistance from the fins is computed using CFD and can be seen in Table 5.

**Table 5 Effect of fins on towing resistance**

| $V_S$ [knots] | Added resistance due to the fins [%] |
|---|---|
| 5 | 16.4 |
| 15 | |

The pressure distribution on the fin can be seen in together with limiting streamlines in Figure 7.

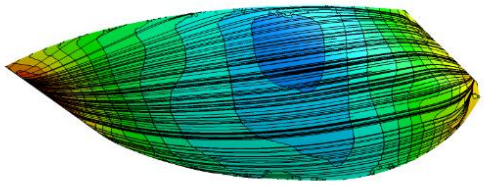

**Figure 7 Pressure and limiting streamlines on portside fin in 5 knots**

### 3.3 Propeller inflow

The propeller inflow is studied by analyzing the nominal wake field, the effective wake and the total wake field and propeller loading. The (axial) wake fields are computed as $1 - U_x/U_\infty$.

The nominal wake field in the propeller centrum can be seen in Figure 8. Average nominal wakefield in the propeller plane is 0.177.

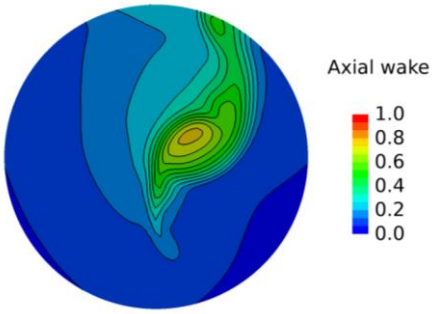


**Figure 8 Nominal wake field in the propeller plane (radius = 1R)**

Propulsion computations were performed in towing mode, yielding effective wake and thrust deduction factor. All propulsion computations were performed with a time step equaling 1° rotation of the propeller.

The effective wake is based on the average load and is computed to be as seen in Table 6.

**Table 6 Effective wake**

| $V_s$ [knots] | Effective wake [-] |
|---|---|
| 5 | 0.02 |

The total wake is shown in Figure 9. In comparison to the nominal wake it can be seen that the wake field is accelerated the least in the same region as the wake is the highest in the nominal wake field, which is expected.

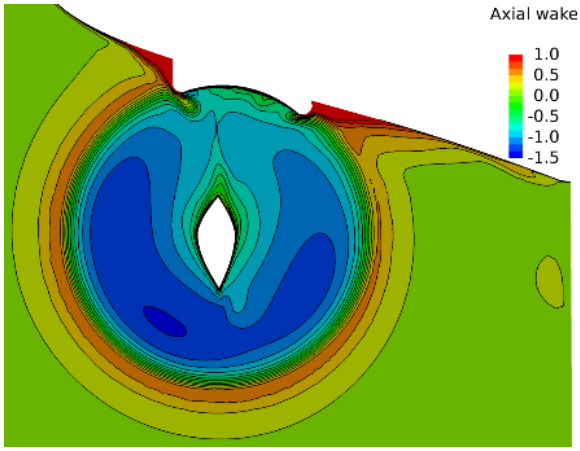


**Figure 9 Total axial wake field 0.5D upstream of propeller (12 O'clock position)**

In 5 knots and towing mode the thrust and torque varies as plotted in Figure 10. The double amplitude for the torque is 3.2% and for thrust the equivalent number is 3.6%. We can here see how the maximum loading occurs about 72° past the 12'O clock position (0° and 90°).

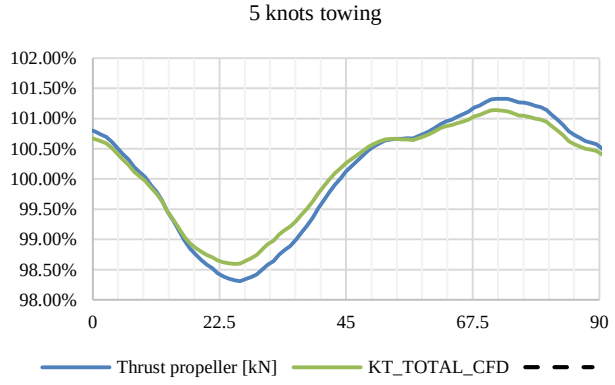


**Figure 10 Thrust and torque variation during one blade passing**

The non-dimensional pressure coefficient is computed as $C_{pn} = (p - \rho g Z - p_{atm})/(0.5\,\rho(nD)^2)$. $C_{pn}$ is shown on the suction- and pressure side of the portside propeller at blade angles of 0°, 30° and 60° degrees. Looking at the pressure side it can be seen that the loading is the highest on the top blade at -30° and 0° degrees blade position, which agrees with the load variation shown in Figure 10 and the nominal wake field in Figure 8.

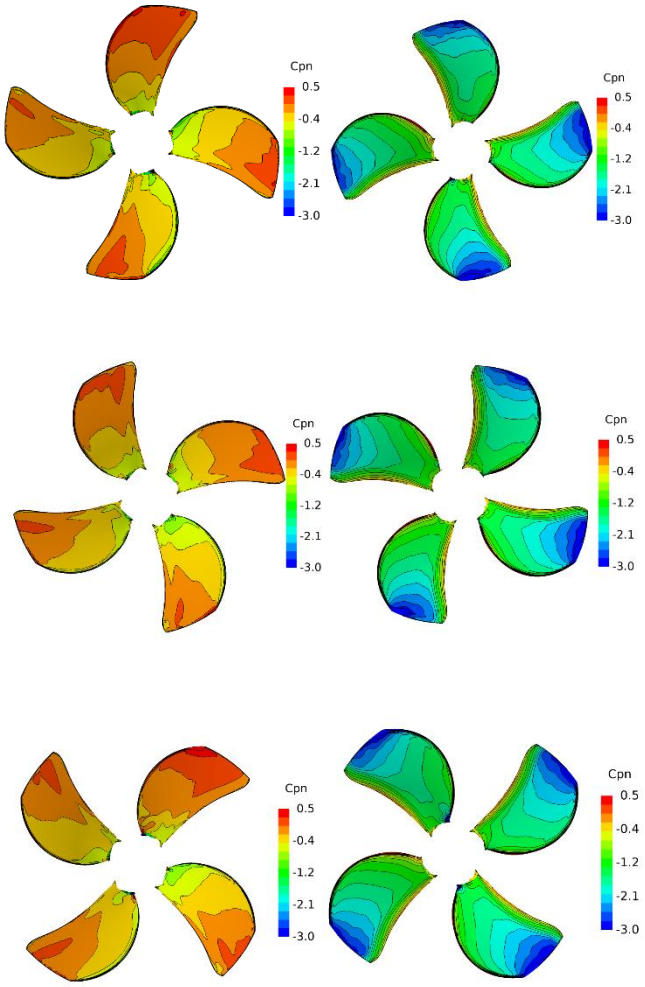


**Figure 11 Cpn on portside propeller blades**

### 3.4 Cavitation in towing mode

The thrust and torque variation can be seen in figure. The excitations are now larger, with a double amplitude for the torque of 5.1% and for thrust 6.0%. Note that the maximum propeller loading now occurs at slightly more than 45° past the 12'O clock position. The minimum loading point occurs at about 10 degrees. The high frequency noise seen in both thrust and torque is suspected to have a numerical background rather than physical.

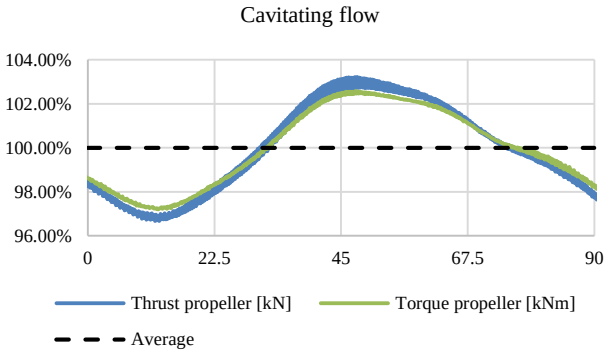


**Figure 12 Thrust and torque variation during one blade passing in cavitating condition**

The cavitation extent is shown on the blades in figure using an isosurface for $\alpha_l = 0.5$ at propeller position of 55°.

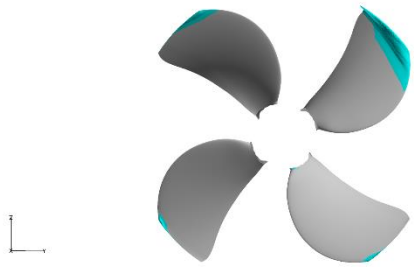

**Figure 13 Cavitation on propeller suction side**

### 3.5 Thrust deduction

The pressure coefficient Cpn is shown on the hull under the water surface (threshold $\alpha_l > 0.5$) in Figure 14. The low pressure on the fin just upstream of the nozzle propeller is a contributor to thrust deduction. This low pressure upstream of the propeller position acts mainly on the fin which means that the thrust deduction can be expected to have a weaker coupling to the hull design than to the fin design. Note that the simulation is mirrored in the visualization environment.

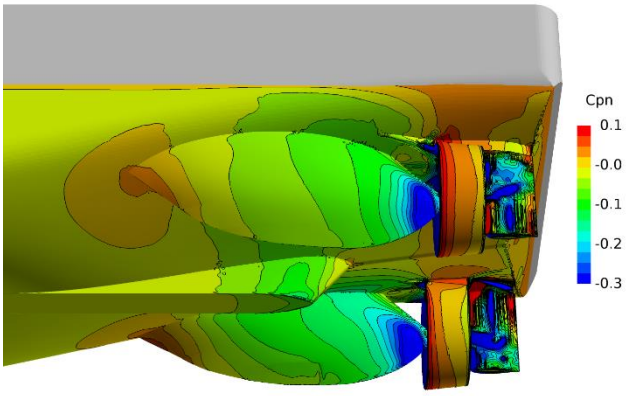


**Figure 14 Pressure on stern**

The thrust deduction factor is shown in Table 7.

**Table 7 Thrust deduction**

| $V_s$ [knots] | Thrust deduction [-] |
|---|---|
| 5 | 0.185 |

### 3.6 Including the fin as thrust deduction

If we instead consider the fin to be a part of the propulsion system, and thereby incorporates the fin resistance as thrust deduction, the thrust deduction becomes 0.19, Table 8. This means that the fin towing resistance is equal to 0.5% of the thrust in towing mode.

**Table 8 Thrust deduction when including the fin resistance as thrust deduction**

| $V_s$ [knots] | Thrust deduction [-] |
|---|---|
| 5 | 0.19 |

## 4 CONCLUSIONS AND FUTURE WORK

The Twin Fin propulsion system has been presented applied on a typical offshore support vessel (OSV). The system consists of a fin, short shaft, propeller and nozzle. The Twin Fin propulsion system manages large propeller diameters due to the robust mechanical parts and the fins protecting the propeller. The gains of increasing the diameter for a highly loaded propeller was shown by an example where a 3.5m propeller was compared to a 4.5m propeller using experimental data. In this example, a bollard pull gain of 23% and in towing mode of 16% was shown. In addition to this, the simple mechanical setup in comparison to e.g azimuth thrusters yields a better mechanical efficiency which would increase the thrust even more.

The added resistance due to the fins was investigated using CFD, where a 16.4% increase was found in towing mode, 5 knots, and 10% in the free running mode, 15 knots. The nominal wake field when including the fin was found to be 0.177 in average in the propeller plane. The propeller hull interaction was further investigated in towing mode. The results shows a smooth circumferential load variation where the double amplitude of the thrust and torque is 3.6% and 3.2% of the mean load, respectively. The cavitating simulation showed an increase in load variation as the double amplitude for thrust and torque was found to be 6.0% and 5.1% of the mean. Furthermore, the load variation in cavitating condition has its maximum and minimum earlier than in wetted condition, with slightly different load variation development. Isosurface of the cavitation shows that significantly more cavitation was found on the blade at 55° position rather than the blade at 55°-90°=-35° position which was not expected from the wetted flow load variation.

The low pressure upstream of the propeller acts on the fin giving rise to thrust deduction. This low pressure mainly acts on the fin and only to a limited extent on the hull, which means that it is expected that the thrust deduction factor which was found to be 0.185can be expected to only have a weak coupling to the hull design. If the fin is considered a

part of the propulsion systems and therefore adds the fin towing resistance to the thrust deduction, the thrust deduction factor increases to 0.19. This means that the towing resistance for the fins is equal to 0.5% of the thrust in towing mode.

Future work should be focused on doing similar in-behind simulations in free running mode, although the towing mode is of greatest interest for this type of vessels. The effective wake field could be determined as well if an open water diagram was generated using CFD. The special treatment of the phases in cavitating condition needs to be validated using experimental data to quantify the discrepancies due to the applied unconventional cavitation approach.

## REFERENCES


Chun, H. H., Park, W. G., and Jun, J. G. (2002), "Experimental and CFD Analysis for Rotor-Stator Interaction of a Water-jet Pump," Proc. 24th Symposium on Naval Hydrodynamics, Fukuoka, Japan, 744-7

Huuva, T. (2008), "Large eddy simulation of cavitating and non-cavitating flows", PhD thesis, Chalmers University of Technology, Gothenburg, Sweden.

Huuva, T. (2014), "The Twin Fin Propulsion Concept". 36th Motorship Propulsion & Emissions Conference, Hamburg, Germany.

Klerebrant Klasson, O. (2011), "A Validation, Comparison and Automation of Different Computational Tools for Propeller Open Water Predictions", MSc thesis, Chalmers University of Technology, Gothenburg, Sweden.

Kunz, R. F., Boger, D. A., Chyczewski, T. S., Stinebring, D. R., Gibeling, H.J., Venkateswaran, S., and Govindan, T. R. (1999), "A Preconditioned Navier Stokes Method for Two-Phase Flows with Application to Cavitation Problems". Proceedings of 14th AIAA CFD Conference., 849-875). Norfolk

Törnros, S. (2013), "Propeller Cavitation Simulation using RANS and OpenFOAM, MSc thesis. Chalmers University of Technology, Gothenburg.


## DISCUSSION

### Question from Kourosh Koushan

What is the overall efficiency of the system (absolute value)?

### Authors Closure

This is very hull dependent, because there is a strong interaction effect between the fin geometry and hull. At

Bollard Pull the resistance of the fin is very low, while at higher speed the resistance of the fin becomes more significant.

### Question from Kourosh Koushan

Have you performed experimental verification of your numerical analysius?

### Authors Closure

No, only full scale tests.

### Question from Dmitriy Ponkratov

Are you planning to perform free sink/trim simulations to further optimize the fin?

### Authors Closure

Yes, there is a plan to also include this.